

## **Crumpled Fibrous Graphdiyne Network Decorated Metal-Organic Framework: A Promising Heterostructure for Improved Energy Storage Performance**

Zahir Abbas <sup>a</sup>, Nissar Hussain <sup>a</sup>, Shaikh M. Mobin <sup>a, b\*</sup>

<sup>a</sup> Department of Chemistry, Indian Institute of Technology Indore, Simrol, Khandwa Road, 453552, India.

<sup>b</sup> Center for Advanced Electronics, Indian Institute of Technology Indore, Simrol, Khandwa Road, 453552, India.

\*Email: [xray@iiti.ac.in](mailto:xray@iiti.ac.in)

## **Materials and Method**

**Materials:** Nickel chloride hexahydrate ( $\text{NiCl}_2 \cdot 6\text{H}_2\text{O}$ ), Dimethyl formamide (DMF), and Methanol, tetrahydrofuran, and trimethylamine Potassium hydroxide (KOH) were purchased from SRL chemicals. Ammonia solutions were purchased from spectrochem. Ni foam and activated carbon were purchased from Global Nanotech Pvt. Ltd. 1, 3, 5 triethyl benzene were purchased from Sigma Aldrich. Deionized water (DI) was used throughout the study. All the chemicals used as received without further purification.

## **Materials characterization**

The morphologies were investigated by a Supra55 Zeiss field emission scanning electron microscope (FESEM) and high-resolution transmission electron microscopy (HR-TEM) was performed using (TEM, JEM F200). Powder X-ray diffraction (PXRD) analysis,  $\text{Cu K}\alpha$  (0.154 nm) monochromatic radiation was used with a Rigaku Smart Lab X-ray diffractometer. X-ray photoelectron spectroscopic (XPS) analysis (XPS, Nexsa, Thermofisher Scientific) incorporating  $\text{Al K}\alpha$  as the source of X-ray. Brunauer–Emmett–Teller (BET) surface area and Barrett–Joyner–Halenda (BJH) distribution determinations were conducted on an Autosorb iQ (Quantachrome Instruments, version 1.11).

## **Electrochemical measurements**

Electrochemical measurements were carried out in the three-electrode system in 2M KOH as electrolyte. 2 mg of active materials were dispersed in 0.5 ml ethanol for 4h to complete the dispersion of the solution and 10  $\mu\text{l}$  nafion was added. The active material was drop cast on the Ni foam ( $1 \times 1\text{ cm}$ ). The prepared electrode was completely dried and used for further studies. The electrochemical techniques such as cyclic voltammetry (CV), galvanostatic discharge/charge (GCD), and electrochemical impedance spectroscopy (EIS). All the electrochemical tests were carried out by using an Autolab instrument. The efficiency evaluation was discussed as follows.

## **Device preparation**

The asymmetric supercapacitor device was fabricated using MOF@GDY as the positive electrode (3 mg), activated carbon as the negative electrode (3 mg), PVA/KOH polymer gel electrolyte as the electrolyte, cellulose paper as the separator, and carbon paper as the current collector. The device was assembled to form a sandwich-like structure. The fabricated device was charged with a 300 mAh AC adapter and for practical applicability used to power a red-

colored LED. Furthermore, the efficiency of the device was tested by using CV, GCD, and EIS measurements.

### Efficiency evaluation

The specific capacitance of as-synthesized electrode materials was evaluated through the GCD curves by using the following relation

$$C_s = \frac{I \times \Delta t}{m \times \Delta V} \quad 1$$

where  $I/m$ ,  $\Delta t$ , and  $\Delta V$  represent current density, discharge time, and the potential range of the GCD profile, respectively.

Furthermore, the energy density (E) and power density (P) of the asymmetric device (ASC) were calculated by the following relations.

$$E = \frac{C_s}{2 \times 3.6} \Delta V^2 \quad 2$$

$$P = \frac{E}{\Delta t} \times 3600 \quad 3$$

where  $C_s$ ,  $\Delta V$ , and  $\Delta t$  indicate the specific capacitance, potential window, and discharge time of the GCD profile, respectively.

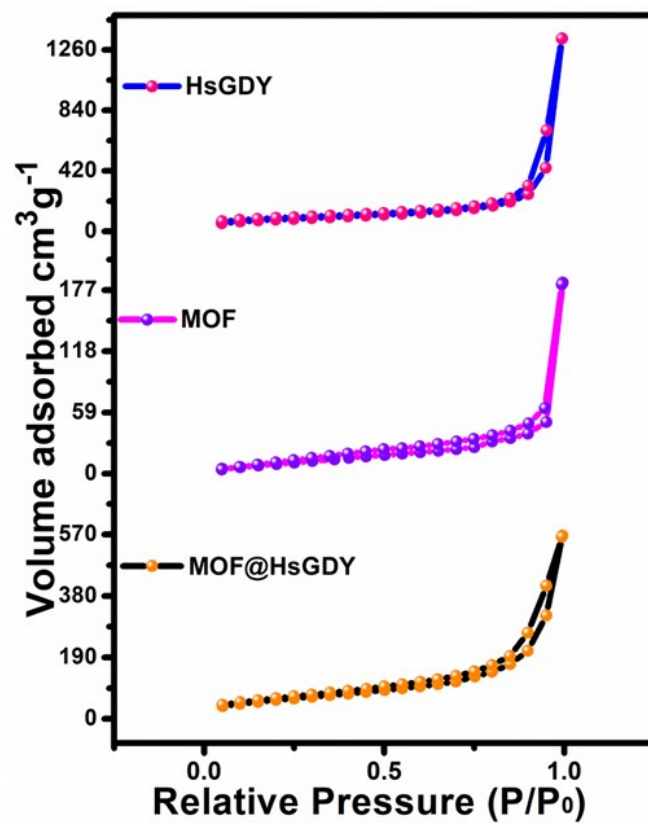


**Fig. S1.** BET surface area analysis of HsGDY, MOF, and MOF@HsGDY.

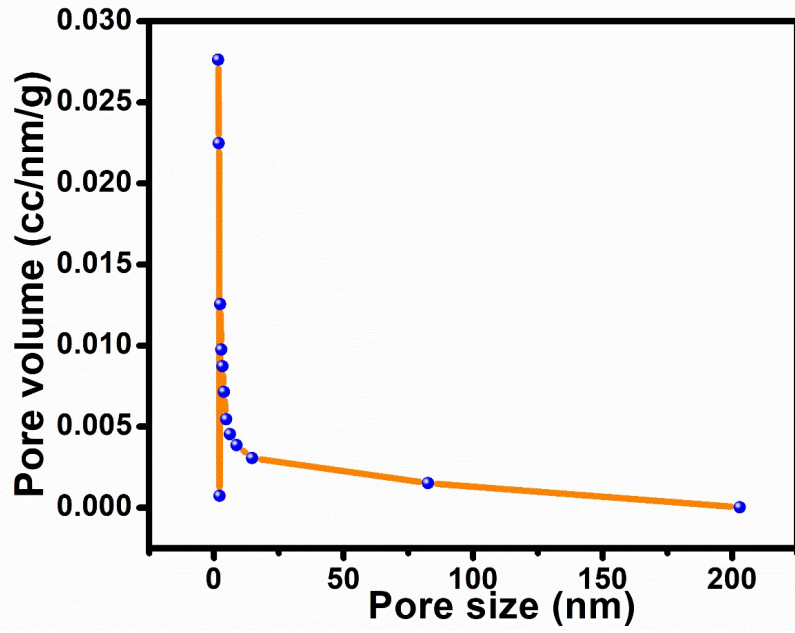


**Fig. S2.** Pore diameter analysis of HsGDY.

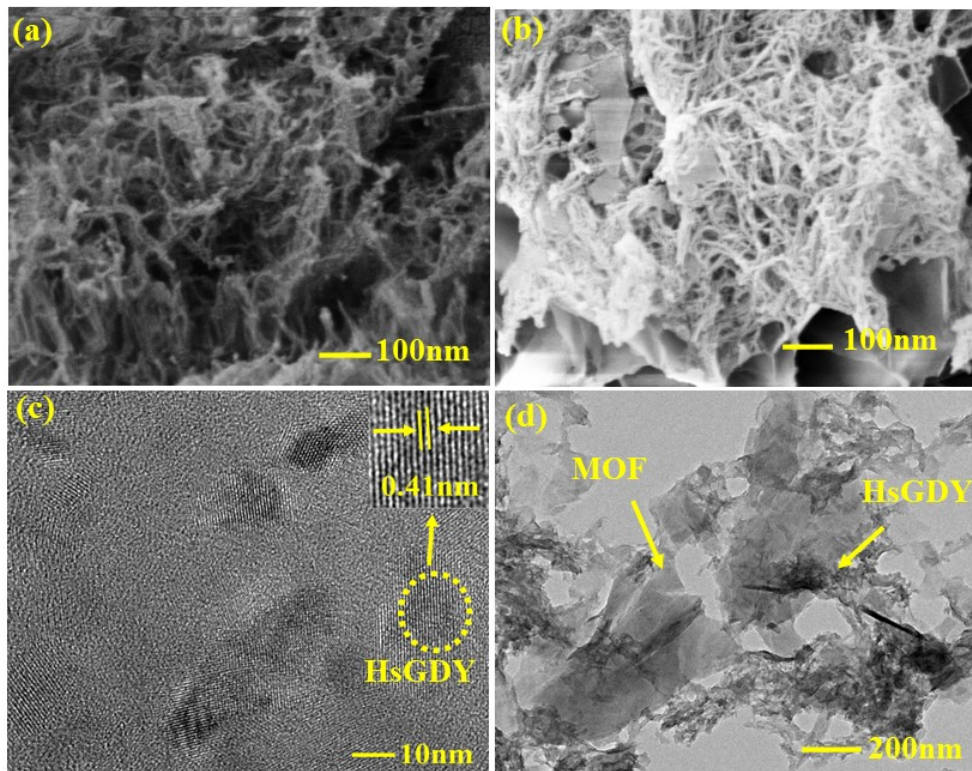


**Fig. S3.** (a) SEM analysis of HsGDY (b) MOF@HsGDY: HR-TEM analysis of (c) GDY and (d) MOF@HsGDY.

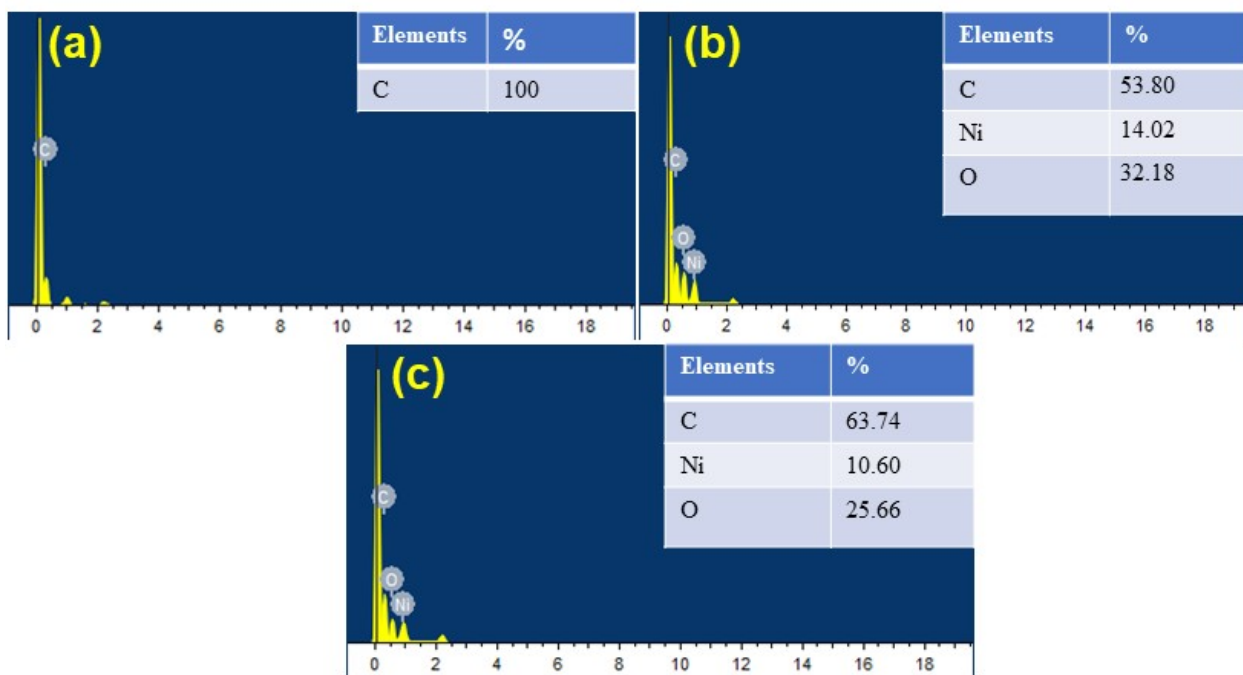


**Fig. S4.** (a) EDX of graphdiyne (b) EDX of MOF (c) MOF@HsGDY.

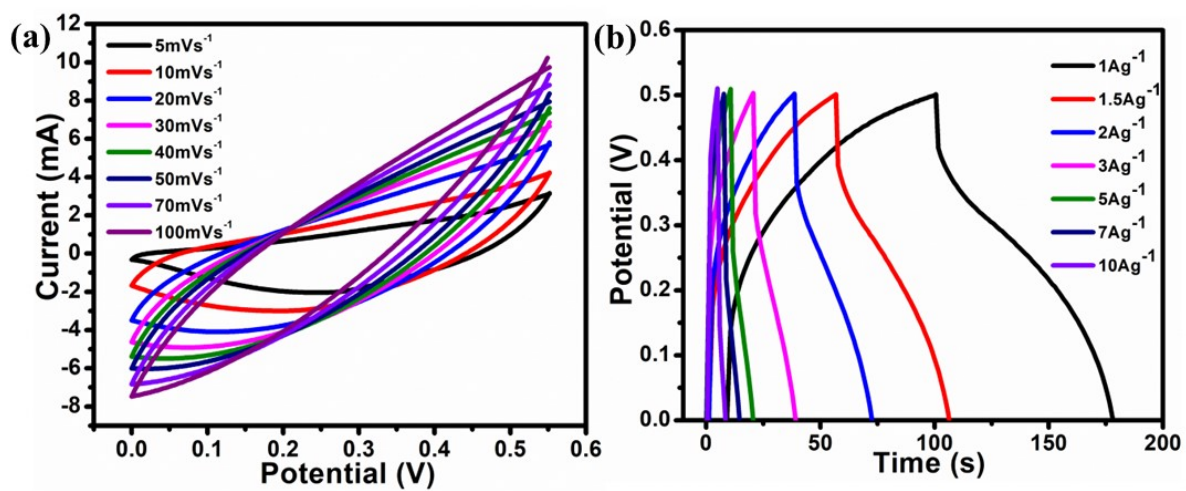


Fig. S5. (a) CV curve of pure HsGDY and (b) GCD analysis of HsGDY.

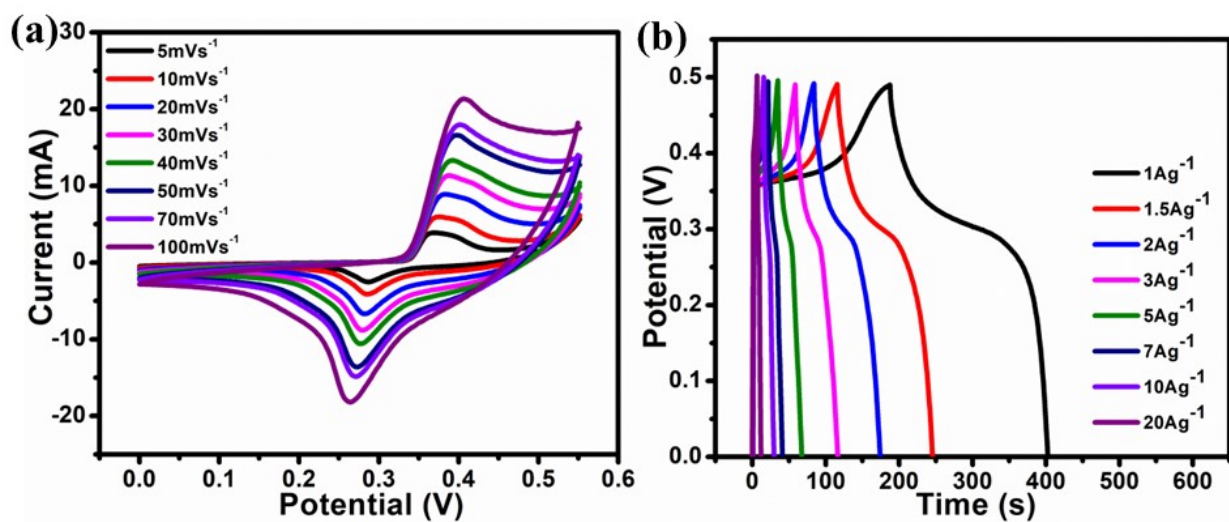
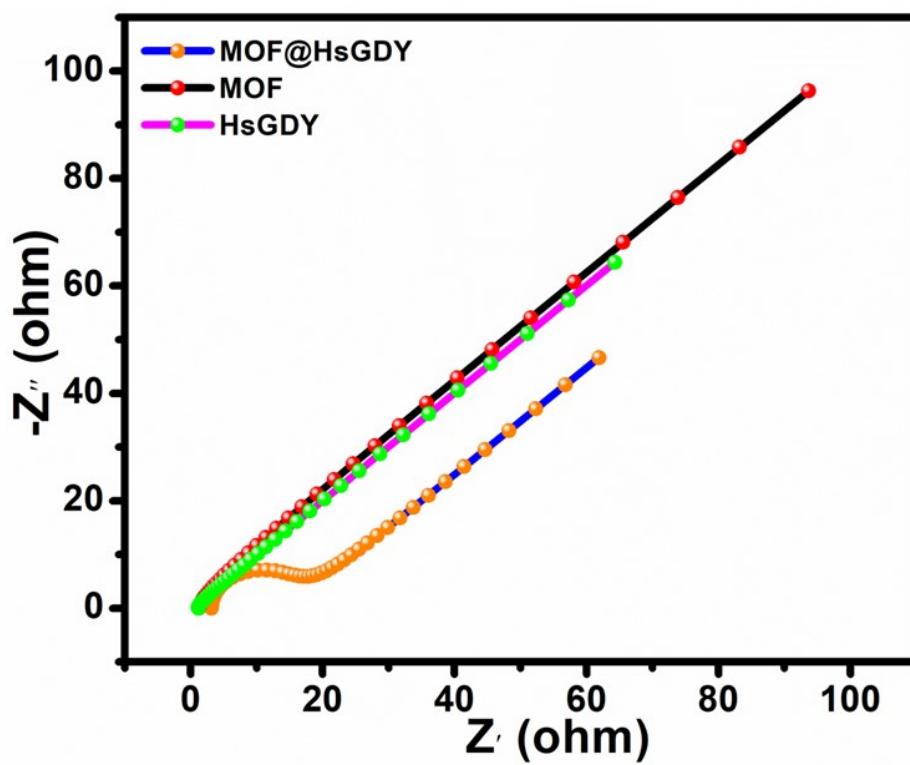


Fig. S6. (a) CV curve of pure Ni-MOF (b) GCD analysis of Ni-MOF.





**Fig. S7.** EIS analysis of MOF, GDY, and MOF@GDY.

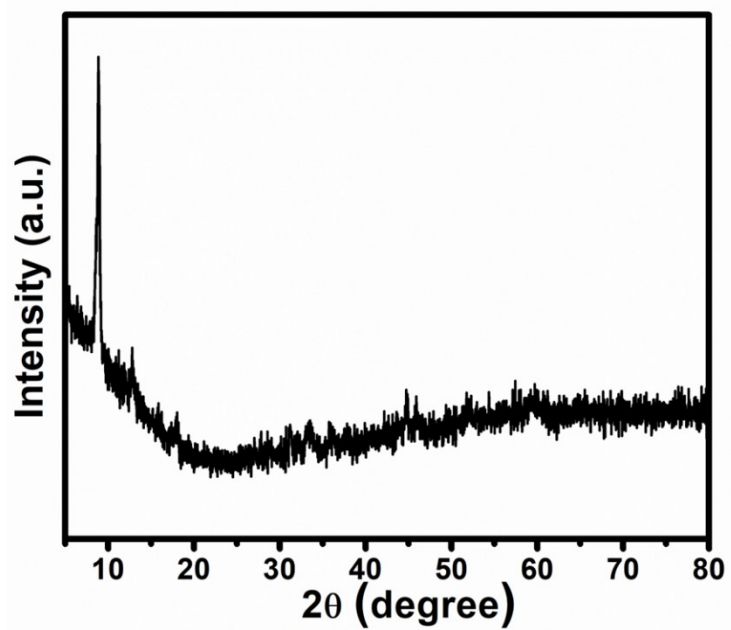


Fig. S8. XRD analysis of MOF@HsGDY post electrochemical test.

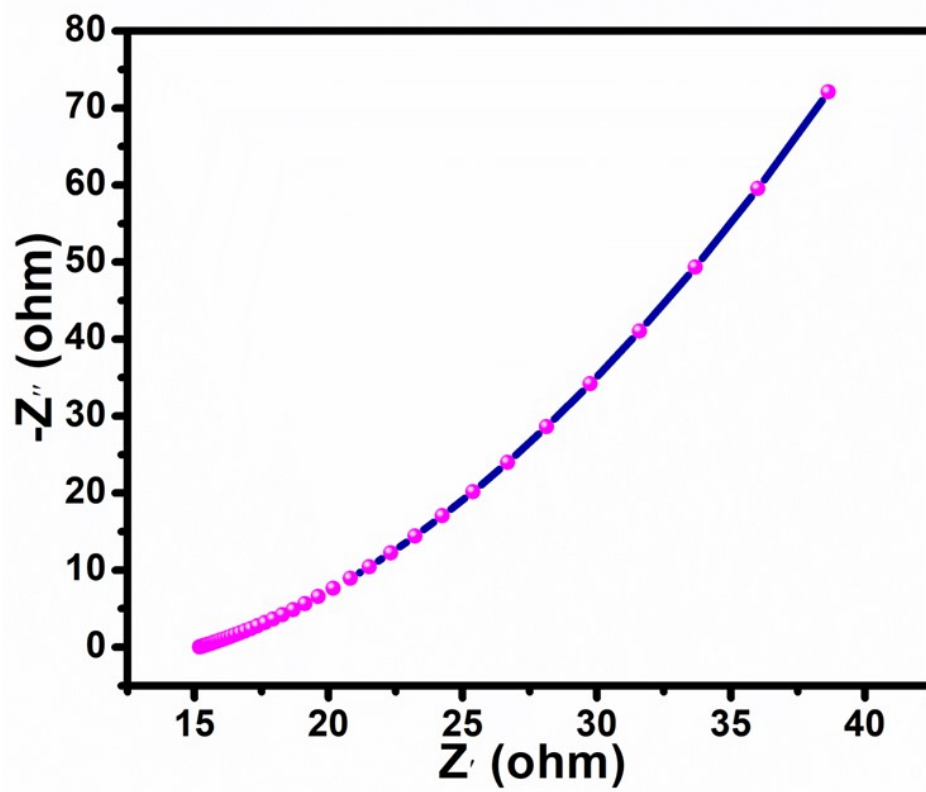


Fig. S9. EIS of MOF@HsGDY//AC ASC device.

**Table S1.** Comparison of energy storage performance of prepared MOF@GDY with other recently reported literature on GDY and MOF-2D hybrid materials.

S.no.	Electrode materials	Specific Capacitance	Cycling stability	References
1	MXene/Graphdiyne nanotube	337.4 Fg <sup>-1</sup> at 1Ag <sup>-1</sup>		1
2	NiCo <sub>2</sub> O <sub>4</sub> @GDY	200.9 Fg <sup>-1</sup> at 1Ag <sup>-1</sup>	97.7% after 10,000 cycles	2
3	Triazene-GDY	250 Fg <sup>-1</sup> at 0.1Ag <sup>-1</sup>	97.6% after 10,000 cycles	3
4	Lamelliform-GDY	137.8 Fg <sup>-1</sup> at 1Ag <sup>-1</sup>	81.28% after 11,000 cycles	4
5	Ti <sub>3</sub> C <sub>2</sub> T <sub>X</sub> /ZIF-67/CoV <sub>2</sub> O <sub>6</sub>	264.5 F g <sup>-1</sup> at 1 A g <sup>-1</sup>	94.4% after 4000 cycles	5
6	N-doped graphdiyne	250 Fg <sup>-1</sup> at 0.2Ag <sup>-1</sup>	95.6% after 3000 cycles	6
7	3D GDY-NCNTs	679 F g <sup>-1</sup> , 2 mV s <sup>-1</sup>	116% after 10000 cycles	7
8	MOF derived NPC-rGO	334 F g <sup>-1</sup> 5 mVs <sup>-1</sup>	97.24% after 10,000 cycles	8
9	Graphene acid@ UiO66-NH <sub>2</sub> MOF	651 F g <sup>-1</sup> at 1 A g <sup>-1</sup>	88% after 10,000 cycles	9
10	N/S-co-doped graphene-like carbon	335.1 F g <sup>-1</sup> at 1 A g <sup>-1</sup>	96% after 10,000 cycles	10
<b>11</b>	<b>MOF@HsGDY</b>	<b>982 F g<sup>-1</sup> at 1 A g<sup>-1</sup></b>	<b>94% after 10,000 cycles</b>	<b>This Work</b>

## References:

- 1 Y. Wang, N. Chen, Y. Liu, X. Zhou, B. Pu, Y. Qing, M. Zhang, X. Jiang, J. Huang, Q. Tang, B. Zhou and W. Yang, *Chemical Engineering Journal*, 2022, **450**, 138398.
- 2 X. Zhai, H. Pan, F. Wang, X. Gao, Z. Xiong, L. Li, Q. Chang, S. Cheng, Z. Zuo and Y. Li, *ACS Appl. Mater. Interfaces*, 2022, **14**, 18283–18292.
- 3 Y. Yue, Y. Xu, F. Kong, Q. Li and S. Ren, *Carbon*, 2020, **167**, 202–208.
- 4 G. Liu, G. Wang and Z. Jin, *Electrochimica Acta*, 2023, **464**, 142866.
- 5 C. Liu, Y. Bai, W. Li, F. Yang, G. Zhang and H. Pang, *Angewandte Chemie International Edition*, 2022, **61**, e202116282.
- 6 H. Shang, Z. Zuo, H. Zheng, K. Li, Z. Tu, Y. Yi, H. Liu, Y. Li and Y. Li, *Nano Energy*, 2018, **44**, 144–154.
- 7 E. Xing, R. Cui, X. Guo, J. Liu, D. Wang, Y. Chai, X. Wang, Y. Chen, J. Dong and B. Sun, *ACS Appl. Mater. Interfaces*, 2024, **16**, 23305–23313.
- 8 N. Kumar, N. Bansal, Y. Yamauchi and R. R. Salunkhe, *Chem. Mater.*, 2022, **34**, 4946–4954.
- 9 K. Jayaramulu, M. Horn, A. Schneemann, H. Saini, A. Bakandritsos, V. Ranc, M. Petr, V. Stavila, C. Narayana, B. Scheibe, Š. Kment, M. Otyepka, N. Motta, D. Dubal, R. Zbořil and R. A. Fischer, *Advanced Materials*, 2021, **33**, 2004560.
- 10 R. Chen, H. Tang, P. He, W. Zhang, Y. Dai, W. Zong, F. Guo, G. He, and X. Wang, *Advanced Functional Materials*, 2023, **33**, 2212078.